Magnetic vortex nucleation modes in static magnetic fields

Marek Vaňatka, (iD) Michal Urbánek, (iD) Roman Jíra, et al.

View Online   Export Citation   CrossMark

ARTICLES YOU MAY BE INTERESTED IN

Magnetic vortex nucleation modes in static magnetic fields

Marek Vaňatka,[1,a] Michal Urbánek,[1,2,b] Roman Jíra,[2] Lukáš Flajšman,[1]
Meena Dhankhar,[1] Mi-Young Im,[3,4] Jan Michalička,[1] Vojtěch Uhlíř,[1]
and Tomáš Šikola[1,2]

[1]*CEITEC BUT, Brno University of Technology, Purkyňova 123, 612 00 Brno, Czech Republic*
[2]*Institute of Physical Engineering, Brno University of Technology, Technická 2, 616 69 Brno, Czech Republic*
[3]*Center for X-ray Optics, Lawrence Berkeley National Laboratory, Berkeley, California 94720, USA*
[4]*Department of Emerging Materials Science, DGIST, Daegu 42988, Korea*

The magnetic vortex nucleation process in nanometer- and micrometer-sized magnetic disks undergoes several phases with distinct spin configurations called the nucleation states. Before formation of the final vortex state, small submicron disks typically proceed through the so-called C-state while the larger micron-sized disks proceed through the more complicated vortex-pair state or the buckling state. This work classifies the nucleation states using micromagnetic simulations and provides evidence for the stability of vortex-pair and buckling states in static magnetic fields using magnetic imaging techniques and electrical transport measurements. Lorentz Transmission Electron Microscopy and Magnetic Transmission X-ray Microscopy are employed to reveal the details of spin configuration in each of the nucleation states. We further show that it is possible to unambiguously identify these states by electrical measurements via the anisotropic magnetoresistance effect. Combination of the electrical transport and magnetic imaging techniques confirms stability of a vortex-antivortex-vortex spin configuration which emerges from the buckling state in static magnetic fields. © *2017 Author(s). All article content, except where otherwise noted, is licensed under a Creative Commons Attribution (CC BY) license (http://creativecommons.org/licenses/by/4.0/).* https://doi.org/10.1063/1.5006235

Magnetic vortices are flux-closing magnetization configurations known to occur in micro- or nano-size disks or polygons fabricated from soft magnetic materials like Permalloy. They consist of a magnetization curling in the disk plane and of a vortex core located at the center, where the magnetization points perpendicular to that plane.[1–3] A vortex state is described by two independent parameters: the circulation, and polarity. The circulation is defined by the sense of the magnetization curling (clockwise, $c = -1$ or counterclockwise, $c = 1$) while the polarity is given by the magnetization direction in the vortex core (pointing up, $p = 1$ or down, $p = -1$). The product cp defines the vortex handedness which can be either right-handed ($cp = 1$) or left-handed ($cp = -1$). The four distinct combinations of c and p in a single element promise possible applications related to multibit memory cells.[4,5] Other applications include logic circuits[6] or radio-frequency devices[7,8] using gyrotropic excitation of the vortex core with eigenfrequencies typically on the order of hundreds of MHz. Recent studies have shown magnetic vortices as spin wave emitters[9] using two antiferromagnetically coupled disks in a heterostructure providing a system with much higher eigenfrequencies when compared to a single magnetic disk with a vortex state.

Controlling the vortex states by switching the vortex polarity or circulation has been shown both in dynamic[10–14] and static[15–19] regimes. The circulation switching requires annihilation of the

---

[a]marek.vanatka@ceitec.vutbr.cz

[b]urbanek@fme.vutbr.cz

vortex by displacing the vortex core out of the magnetic disk, followed by nucleation of a new vortex in decreasing external field. The resulting state of the newly nucleated vortex can be controlled by asymmetric disk geometry[20–22] or by symmetry breaking arising from the Dzyaloshinskii–Moriya interaction.[23] The nucleation process, i.e. the evolution of magnetization between the fully saturated state and the fully nucleated vortex, proceeds via different spin configurations, called the nucleation states. These configurations have been predicted by micromagnetic simulations, which were matched to experimentally acquired hysteresis loops.[18,19]

Here we use magnetic imaging to study the nucleation process of the magnetic vortices in slowly decreasing magnetic fields. Fig. 1 shows the three nucleation states obtained by micromagnetic simulations using the Object Oriented Micromagnetic Framework[26] (OOMMF) with the following parameters: a cell size of $(4 \times 4 \times 4)$ nm^3, saturation magnetization $M_s = 800$ kA/m and exchange constant $A = 13$ pJ/m. The first nucleation state, the C-state,[15] is shown in Fig. 1(a). It consists of spins following the shape of the C letter in order to decrease the dipolar energy compared to the disk in saturation. This state is common for small disks (approximately for diameters $D < 400$ nm and thicknesses $t < 20$ nm). In this work, we focus on two other nucleation states that can be found in larger disks: the vortex-pair state[24,27] and the buckling state[15,19,25] [Fig. 1(b) and Fig. 1(c), respectively]. These states were studied by micro-Hall magnetometry[18] and anisotropic magnetoresistance[19,25] (AMR) measurements and compared to micromagnetic simulations. The vortex-pair state and the buckling state were previously imaged by Lorentz Transmission Electron Microscopy[24] (LTEM) and Magnetic Force Microscopy[25] (MFM), respectively. However, some details of the buckling state configuration could not be captured, as the MFM technique does not probe the spin structure directly. Comprehensive study of the vortex nucleation processes using a combination of magnetic microscopies and electric transport measurements allows for studying the whole nucleation sequences in detail and led us to identification of a novel spin configuration emerging from the buckling state – the vortex-antivortex-vortex triplet (VAV triplet).

The vortex-pair state is favored in intermediate disks with diameters $D > 400$ nm and thicknesses $t < (120,000 \pm 24,000)$ nm$^2/D$. The constant $(120,000 \pm 24,000)$ nm^2 was extracted from a simple t-D phase diagram by fitting the boundary between the vortex-pair and buckling states. The identification of vortex-pair and buckling state stability regions was done by the analysis of LTEM images of arrays
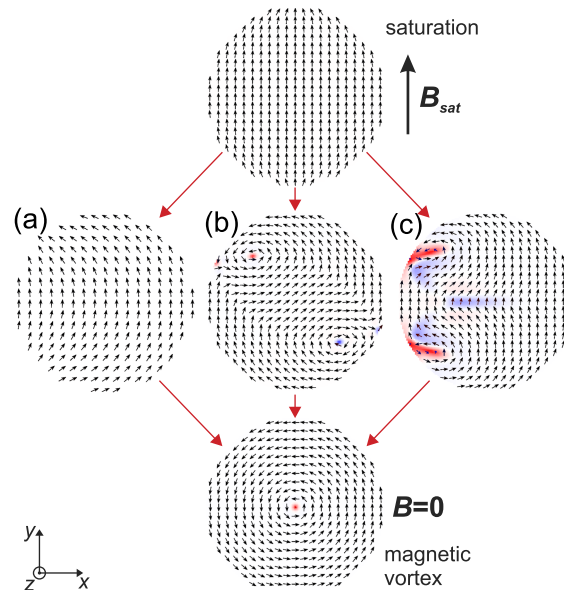

FIG. 1. Magnetic vortex nucleates upon the field decrease from saturation proceeding through the nucleation states visualized by micromagnetic simulations: (a) the C-state ($B = 10$ mT, $D = 200$ nm, $t = 16$ nm), (b) the vortex-pair state ($B = 32$ mT, $D = 1$ μm, $t = 50$ nm), and (c) the buckling state ($B = 60$ mT, $D = 1$ μm, $t = 100$ nm). The blue-white-red color scale represents the perpendicular component of magnetization.

of different sized disks with thicknesses ranging from 20 nm to 100 nm and diameters ranging from 500 nm to 4 μm. However, the crossover between the vortex-pair state and the buckling state is continuous and for each disk geometry in this work we found both states with an increasing probability of finding the buckling state in large disks. The vortex-pair state consists of two vortex cores around which the magnetization is curling in opposite sense (opposite circulations). Micromagnetic simulations show that in zero out-of-plane magnetic field the two cores of the vortex-pair state have opposite polarities (giving the same handedness for both vortices of the pair). Upon the in-plane field decrease, the cores move towards each other decreasing the net magnetization along the field direction until they annihilate and a single vortex core is formed in the disk. As the polarity and circulation of the two competing vortices are opposite, the final vortex state will be random for symmetry reasons. However, in real samples this is difficult to realize because the geometrical symmetry can be broken due to lithographic imperfections and surface roughness of the substrate. In thin disks (e.g. 15 nm[24]) the two vortex cores never unpin from the disk boundary before the vortex is nucleated. The in-plane magnetization then forms the letter S so the vortex-pair state is also called the S-state.[15,24]

The buckling state is favored in large disks. The characteristic features of the buckling state are three Bloch domain walls with in-plane magnetization curling around them [see Fig. 1(c)]. The three walls can have different combinations of the out-of-plane magnetization directions. When the applied field is decreased, the three domain walls move towards each other until a vortex state is formed. The buckling state has a lower symmetry than the vortex-pair state and the in-plane magnetization shape indicates the final circulation of the vortex – in case of Fig. 1(c) the circulation will become counterclockwise. Even though the situation is less evident for the final polarity state, the simulations show that the m_z components at the disk edge will become dominant over those at the disk center – in case of Fig. 1(c) the vortex core polarity will be defined by the m_z component of the red domains.

Experimental verification of the nucleation states was carried out for Permalloy disks with diameters ranging from 500 nm to 4 μm and thicknesses ranging from 20 nm to 100 nm. The disks were fabricated by electron beam lithography, electron beam evaporation and lift-off process on 30-nm-thick and 200-nm-thick SiN membranes suitable for the LTEM and Magnetic Transmission X-ray Microscopy (MTXM), respectively. For the AMR measurements we used undoped Si (100) as a substrate and the disk fabrication was followed by a second lithography step in which a pair of Au contacts was fabricated [with geometry schematically shown in Fig. 3(a)] in order to establish electrical connections to the disk. The spacing between the contacts was equal to one disk radius.

The LTEM images (Fresnel imaging by defocusing) of the nucleation states were acquired using a FEI Titan Themis 60-300 TEM at the accelerating voltage of 300 kV. The results are shown in the upper row of Fig. 2. This method does not image the magnetization inside of the sample directly, but only reveals the domain wall structure. The images of neighboring domains shift towards each other or apart from each other due to opposite Lorentz forces acting on the electrons, thus creating a positive or negative overlap which yields white or black contrast, respectively.[28] This ambiguity can be overcome by performing micromagnetic simulations of the corresponding magnetization states and comparing the calculated LTEM contrast to the measured data. We used Micromagnetic Analysis to Lorentz TEM Simulation[29] (MALTS) to provide the comparison between the acquired images and the simulations. The images of LTEM contrast calculated by MALTS are in the middle row of Fig. 2 and the source magnetization distributions simulated by OOMMF in the bottom row of Fig. 2. The external magnetic field needed for vortex annihilation and subsequent gradual nucleation is applied by the TEM objective lens (which is normally turned off in the Lorentz mode). As this field is oriented along the microscope optical axis, the sample was tilted by 30 degrees to gain an in-plane component of the magnetic field. The tilt also results in elliptical projections of the disks. The out-of-plane component of the magnetic field imposes the out-of-plane magnetization direction of the emerging vortex cores and Bloch domain walls, as confirmed by the simulations. LTEM images show a good agreement between the simulated and measured magnetic contrast for both the vortex-pair state [Figs. 2 (a) and 2(b)] and the buckling state [Figs. 2 (c) and 2(d)]. For comparison we show a simulation of the C-state in a 200-nm-wide and 16-nm-thick disk [Fig. 2(e)], which does not show contrast in LTEM. The final vortex state at zero field is shown in Fig. 2 (f).
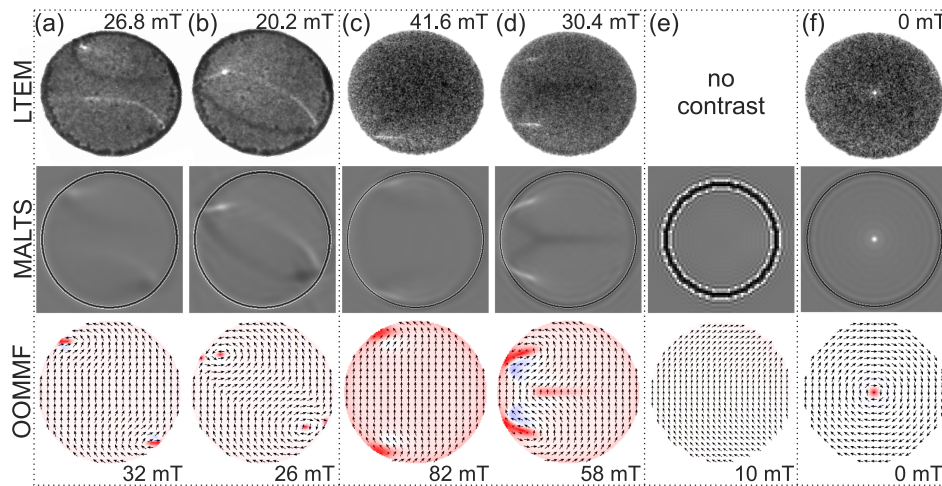
FIG. 2. Simulation and LTEM imaging of vortex nucleation states in magnetic field. The sample was tilted by 30° and the indicated field values are the in-plane field components. Top row: LTEM observation; middle row: LTEM contrast simulated from the spin configurations shown in the bottom row: OOMMF micromagnetic simulations taking into account both in-plane and out-of-plane components of the magnetic field. The blue-white-red color scale represents the perpendicular component of magnetization. Columns: (a), (b) two consecutive configurations showing the formation of the vortex-pair state in a 2-μm-wide and 40-nm-thick disk. (c), (d) formation of the buckling state in a 2-μm-wide and 100-nm-thick disk. (e) Simulations of the C-state in a 200-nm-wide and 16-nm-thick disk which does not show magnetic contrast in LTEM. (f) Final vortex state.

The vortex-pair state nucleation process consists of two steps indicated in Figs. 2(a) and 2(b). The LTEM image in Fig. 2(a) is characterized by two lines (in-plane domain walls with black or white contrast) separating the three main domains defining the in-plane magnetization in the disk. Additionally, we can observe two intense spots at the disk boundary where one of them is lighter and the other one darker than the background. They represent Bloch domain walls featuring a larger magnetization curl (i.e. higher contrast). Upon decreasing the field, the white and black lines move closer to each other until the Bloch domain walls unpin from the disk boundary into two standalone vortex cores yielding the spin configuration of the vortex-pair state in Fig. 2(b). Further field decrease leads to the formation of a single vortex. In case of the buckling state [Fig. 2(c) and 2(d)], the nucleation process is different. When the field decreases below the saturating values, the first step is the formation of Bloch domain walls at the disk boundary yielding bright LTEM contrast in these positions. From this state, the buckling state is formed by moving the two domain walls towards each other, which is accompanied by gradual formation of a third domain wall at the disk center. The LTEM contrast then consists of a typical line passing through the disk center splitting towards the edge where the line bounces off the edge with reversed contrast [from black to white in case of Fig. 2(d)]. Further field decrease leads to the formation of a single vortex with polarity defined by the m_z component of the Bloch walls nucleated at the disk boundary.

The nucleation processes were further detected by measuring the associated resistance changes due to AMR. Considering the experimental geometry presented in Figs. 3(a) and 3(b) with the magnetic field oriented along the *y*-axis, the highest resistance is measured at saturation where the spins are aligned along both the applied field and the current density **j**. Then any other state comes with a lower level of electrical resistance following the AMR law for resistivity: $\rho(\varphi) = \rho_\perp + (\rho_\| - \rho_\perp)\cos^2\varphi$, where φ is the angle between the vector of current density **j** and the vector of magnetization **m**. The OOMMF vector magnetization maps were used to calculate the resistance of consecutive states along the hysteresis loop in order to predict the shape and specific features of the sweeps for the different nucleation processes. The calculation consisted of assigning a resistance value to each simulation cell by following the AMR formula and then connecting all cells together in a grid. The total grid resistance was obtained by calculating the resistance of each row of cells as of parallel resistors and then adding up the resistances of all rows as resistors in series. We assumed that
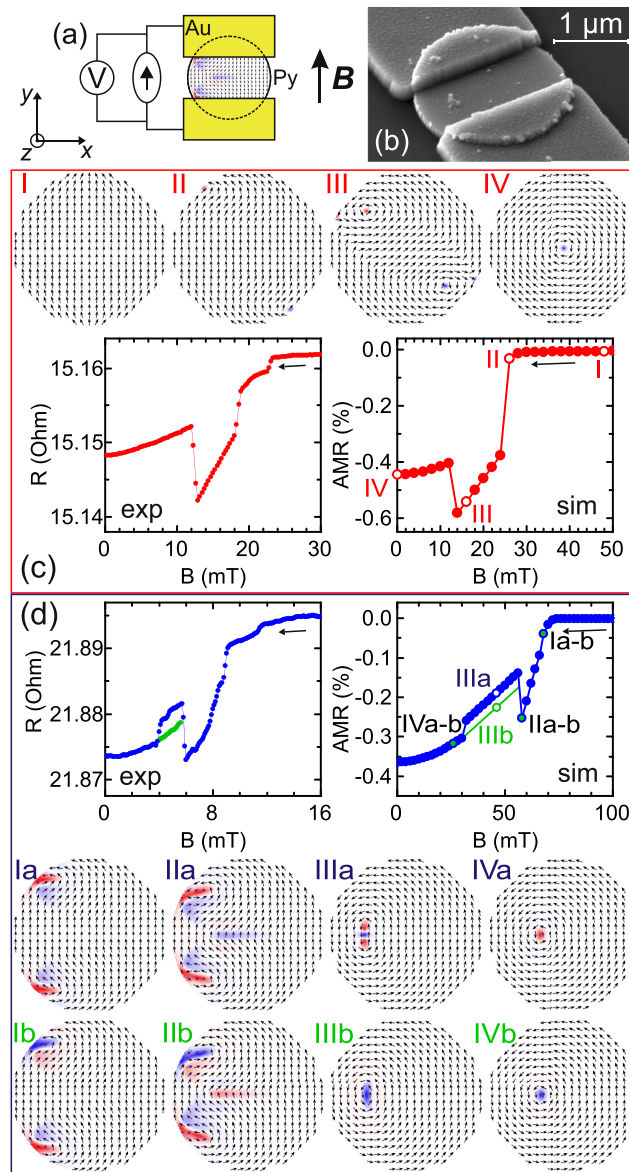
FIG. 3. Modeling and measurement of the AMR data probing the vortex nucleation pathways. (a) Schematics of the sample geometry with electrical connections. (b) SEM micrograph of the Permalloy disk with gold contacts prepared by a two-step lithography process. (c) Simulated and experimental AMR data for a 2-μm-wide and 75-nm-thick disk. The vortex nucleation proceeds through the vortex-pair state. Selected simulation snapshots are indicated (I-IV). (d) Simulated and experimental AMR data for a 4-μm-wide and 50-nm-thick disk. The vortex nucleation proceeds through the buckling state with two variations: a blue curve corresponding to the formation of a VAV triplet (simulated snapshots Ia-IVa) and a green curve where a single vortex is formed directly (simulated snapshots Ib-IVb).

the current is flowing only between the gold contacts [see Fig. 3(a)] with a constant current density j along the y-axis. The two constants $\rho_\perp$ and $\rho_\parallel$ were measured for a continuous Permalloy film gaining values $\rho_\perp = 7.40 \cdot 10^{-7} \Omega$m and $\rho_\parallel = 7.50 \cdot 10^{-7} \Omega$m.

Fig. 3(c) shows the simulated and experimental AMR data for vortex nucleation through the vortex-pair state. The magnetic field was swept in the direction from positive to negative field values. The simulated data in Fig. 3(c) show an abrupt drop of resistance at 24 mT (point II) where the vortex-pair state is formed in the disk and then the resistance decreases linearly (point III) upon further lowering of the field. This is associated with the motion of the two cores of the vortex-pair state towards each other until the two cores annihilate into a single vortex state at 12 mT, which leads

to an abrupt increase of the resistance. The following curve represents the reversible displacement of the single vortex core in magnetic field (point IV). The experimental data in Fig. 3(c) show qualitative agreement with the simulation. They quantitatively differ in the sharpness of the resistance drop upon nucleation, the size of the dip, and the absolute values of the magnetic field. The first difference can be explained by the pinning of magnetization (also observed during the LTEM imaging) at the initial state of nucleation. The size of the dip is influenced by the exact placement of the gold contacts (which may slightly differ between the experiment and simulation) and by the assumption of constant current density within the disk. The experimental values of the nucleation and annihilation fields are lower than the simulated values in agreement with previous observations[18,24] and may be explained by the edge roughness and oxidation leading to deteriorations of the magnetic properties of the disk material[14] and by temperature effects.[30,31]

The AMR data in Fig. 3(d) show similar general behavior compared to the data in Fig. 3(c) but two main differences allow us to associate it with the buckling state nucleation process. The first difference is in the initial part of the nucleation process where the resistance decreases gradually (between points I and II), following the gradual formation of the buckling state all the way from saturation. The other difference is in the depth of the resistance dip relative to the resistance of the vortex state at zero field. The dip is shallower in case of nucleation via the buckling state and it does not drop below the resistance level at zero field as in the case of nucleation via the vortex-pair state. The nucleation occurs after point II, where the resistance suddenly increases. From this point, based on a comparison with micromagnetic simulations, the nucleation can proceed either directly to a single vortex [simulated snapshots Ib-IVb in Fig. 3d], or the magnetization can form a VAV triplet [simulated snapshots Ia-IVa in Fig. 3d] as an intermediate state. The nucleation path depends on the "polarity" (i.e. out-of-plane component of magnetization) of the Bloch domain walls nucleating on the side of the disk. If the domain walls have the same polarities at the disk boundary and the domain wall at the disk center has an opposite polarity, the nucleation proceeds via the VAV triplet [Fig. 3(d), simulated images IIa-IIIa]. If the boundary domain walls have opposite polarities or if all three walls have the same polarities, the nucleation proceeds directly into a single vortex core [Fig. 3(d), simulated images IIb-IIIb]. These two states are distinguishable in the AMR data, as the VAV triplet has a higher resistance than a single vortex (compare points IIIa and IIIb). The VAV triplet is stable in a field range of a few mT and after further field decrease, it annihilates into a single vortex core resulting in a small drop in the AMR data. When performing multiple measurements on the same disk, we observed that nucleation via the VAV triplet occurred less frequently compared to direct nucleation into a single vortex core. This can be attributed to two aspects: (i) the buckling state has a lower energy with alternating polarities of the boundary domain walls and (ii) the VAV triplet has a higher energy when compared to the vortex state with a single core at the same magnetic field. Furthermore, pinning at the edge roughness lowers the symmetry of the nucleation states, which was observed by LTEM imaging (see Fig. 2). This may suppress nucleation of the VAV structure which requires a higher symmetry of the initial spin configuration.

As the out-of-plane component of the applied field sets the domain wall polarities in the same direction, the VAV triplet cannot be captured in LTEM experiments. Therefore, the nucleation from the buckling state both with and without the VAV triplet was imaged using Magnetic Transmission X-ray Microscopy (MTXM) at beamline 6.1.2 (XM-1) at the Advanced Light Source (ALS) in Berkeley, California. Imaging was carried out with a spatial resolution of 25 nm at Fe L3 absorption edge (707 eV). Magnetic contrast at XM-1 is given by X-ray magnetic circular dichroism (XMCD) which is sensitive to the magnetization component parallel to the incoming X-ray beam (i.e. out-of-plane magnetization in our geometry). The MTXM images of a 2-μm-wide and 100-nm-thick Py disk corresponding to the buckling state transformation into the VAV triplet are shown in Fig. 4(a). The nucleation sequence is in a good agreement with the simulated sequence Ia-IVa in Fig. 3(d). The sequence in Fig. 4(b) shows the buckling state evolution with boundary domain walls of opposite polarity [corresponding to points Ib-IVb of Fig. 3(d)] which leads to direct nucleation of a single vortex core.

Complex spin structures emerging from the vortex core were also observed during vortex annihilation by Pulecio et al.[32] The authors used LTEM to image a vortex core close to annihilation, which was surrounded by two line-type domain walls in out-of-plane biasing magnetic field. Although
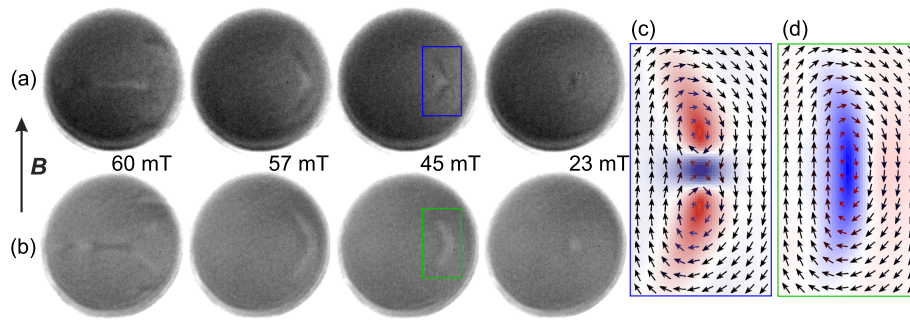
FIG. 4. MTXM images showing nucleation sequences from two variations of the buckling state in a 2-μm-wide and 100-nm-thick disk. (a) Nucleation leading to the VAV triplet. (b) Nucleation leading to a single vortex core. (c) Detail of the VAV triplet (OOMMF simulation). (d) Detail of the vortex core at the same magnetic field as the VAV triplet in (c).

the MTXM (m_z) images shown in Fig. 4 display similar contrast, the components of the VAV spin configuration are different and stable without out-of-plane stabilizing magnetic field.

In conclusion, we studied the nucleation processes of magnetic vortices in Permalloy disks in slowly changing magnetic fields. Two different nucleation states, the vortex-pair state and the buckling state, were confirmed by LTEM imaging in a good agreement with the simulated contrast by MALTS. We have also shown that the distinct spin structures occurring during the nucleation process can be unambiguously detected electrically using the AMR effect. The existence of a stable VAV triplet during vortex nucleation from the buckling state was identified by comparing the AMR measurements to micromagnetic simulations and confirmed by imaging using MTXM. Results of this work could provide a route for applications in the field of magnonics, where the stabilization of more complex spin structures would be the basis for selective RF excitation of spin waves induced either by waveguide-generated magnetic field or spin polarized current. Specifically, the VAV triplet, being a highly confined spin structure, is expected to exhibit eigenfrequencies in the GHz range and can be suitable for spin wave generation using a single magnetic element in contrast to the approach using antiferromagnetically coupled vortices as spin wave emitters.[9]

[1] A. Hubert and R. Schäfer, *Magnetic Domains - The Analysis of Magnetic Microstructures* (Springer, 1998).
[2] R. P. Cowburn, D. K. Koltsov, A. O. Adeyeye, M. E. Welland, and D. M. Tricker, Phys. Rev. Lett. **83**, 1042 (1999).
[3] T. Shinjo, T. Okuno, R. Hassdorf, K. Shigeto, and T. Ono, Science **289**, 930–932 (2000).
[4] S. Bohlens, B. Krüger, A. Drews, M. Bolte, G. Meier, and D. Pfannkuche, Appl. Phys. Lett. **93**, 142508 (2008).
[5] S.-K. Kim, K.-S. Lee, Y.-S. Yu, and Y.-S. Choi, Appl. Phys. Lett. **92**, 22509 (2008).
[6] H. Jung, Y.-S. Choi, K.-S. Lee, D.-S. Han, Y.-S. Yu, M.-Y. Im, P. Fischer, and S.-K. Kim, ACS Nano **6**, 3712 (2012).
[7] V. Novosad, F. Y. Fradin, P. E. Roy, K. S. Buchanan, K. Yu. Guslienko, and S. D. Bader, Phys. Rev. B **72**, 24455 (2005).
[8] N. Hasegawa, S. Sugimoto, H. Fujimori, K. Kondou, Y. Niimi, and Y. Otani, Appl. Phys. Express **8**, 63005 (2015).
[9] S. Wintz, V. Tiberkevich, M. Weigand, J. Raabe, J. Lindner, A. Erbe, A. Slavin, and J. Fassbender, Nat. Nanotech. **11**, 948 (2016).
[10] B. Van Waeyenberge, A. Puzic, H. Stoll, K. W. Chou, T. Tyliszczak, R. Hertel, M. Fähnle, H. Brückl, K. Rott, G. Reiss, I. Neudecker, D. Weiss, C. H. Back, and G. Schütz, Nature **444**, 461 (2006).
[11] M. Kammerer, M. Weigand, M. Curcic, M. Noske, M. Sproll, A. Vansteenkiste, B. Van Waeyenberge, H. Stoll, G. Woltersdorf, C. H. Back, and G. Schuetz, Nat. Commun. **2**, 279 (2011).
[12] R. Hertel, S. Gliga, M. Fähnle, and C. M. Schneider, Phys. Rev. Lett. **98**, 117201 (2007).

[13] V. Uhlíř, M. Urbánek, L. Hladík, J. Spousta, M.-Y. Im, P. Fischer, N. Eibagi, J. J. Kan, E. E. Fullerton, and T. Šikola, Nat. Nanotechnol. **8**, 341 (2013).

[14] M. Urbánek, V. Uhlíř, C.-H. Lambert, J. J. Kan, N. Eibagi, M. Vaňatka, L. Flajšman, R. Kalousek, M.-Y. Im, P. Fischer, T. Šikola, and E. E. Fullerton, Phys. Rev. B **91**, 094415 (2015).

[15] K. Y. Guslienko, V. Novosad, Y. Otani, H. Shima, and K. Fukamichi, Phys. Rev. B **65**, 024414 (2001).

[16] K. Y. Guslienko, V. Novosad, Y. Otani, H. Shima, and K. Fukamichi, Appl. Phys. Lett. **78**, 3848 (2001).

[17] V. Novosad, K. Y. Guslienko, H. Shima, Y. Otani, K. Fukamichi, N. Kikuchi, O. Kitakami, and Y. Shimada, IEEE Trans. Magn. **37**, 2088 (2001).

[18] M. Rahm, M. Schneider, J. Biberger, R. Pulwey, J. Zweck, and D. Weiss, Appl. Phys. Lett. **82**, 4110 (2003).

[19] S. R. Bakaul, B. L. Wu, G. C. Han, and Y. H. Wu, Appl. Phys. Lett. **97**, 042503 (2010).

[20] M.-Y. Im, K.-S. Lee, A. Vogel, J.-I. Hong, G. Meier, and P. Fischer, Nat. Commun. **5**, 5620 (2014).

[21] S. Agramunt-Puig, N. Del-Valle, C. Navau, and A. Sanchez, Appl. Phys. Lett. **104**, 012407 (2014).

[22] G. Shimon, V. Ravichandar, A. O. Adeyeye, and C. A. Ross, Appl. Phys. Lett. **105**, 152408 (2014).

[23] M.-Y. Im, P. Fischer, K. Yamada, T. Sato, S. Kasai, Y. Nakatani, and T. Ono, Nat. Commun. **3**, 983 (2012).

[24] M. Schneider, H. Hoffmann, S. Otto, T. Haug, and J. Zweck, J. Appl. Phys. **92**, 1466 (2002).

[25] T. Wren and O. Kazakova, J. Appl. Phys. **117**, 17E134 (2015).

[26] M. J. Donahue and D. G. Porter, Interag. Rep. NISTIR **6376** (1999).

[27] K. S. Buchanan, P. E. Roy, M. Grimsditch, F. Y. Fradin, K. Y. Guslienko, S. D. Bader, and V. Novosad, Nat. Phys. **1**, 172 (2005).

[28] H. Hopster and H. P. Oepen, *Magnetic Microscopy of Nanostructures* (Springer, 2005).

[29] S. K. Walton, K. Zeissler, W. R. Branford, and S. Felton, IEEE Trans. Magn. **49**, 4795 (2013).

[30] J. Li, J. Shi, and S. Tehrani, Appl. Phys. Lett. **79**, 3821 (2001).

[31] G. Mihajlović, M. S. Patrick, J. E. Pearson, V. Novosad, S. D. Bader, M. Field, G. J. Sullivan, and A. Hoffmann, Appl. Phys. Lett. **96**, 112501 (2010).

[32] J. F. Pulecio, S. D. Pollard, P. Warnicke, D. A. Arena, and Y. Zhu, Appl. Phys. Lett. **105**, 132403 (2014).